© 2016. Published by The Company of Biologists Ltd | Journal of Cell Science (2016) 129, 1490-1499 doi:10.1242/jcs.178467

RESEARCH ARTICLE

The ESCRT-II proteins are involved in shaping the sarcoplasmic reticulum in *C. elegans*

Christophe Lefebvre[1], Céline Largeau[1], Xavier Michelet[2], Cécile Fourrage[1], Xavier Maniere[3], Ivan Matic[3], Renaud Legouis[1,*,‡] and Emmanuel Culetto[1,*,‡]

ABSTRACT

The sarcoplasmic reticulum is a network of tubules and cisternae localized in close association with the contractile apparatus, and regulates Ca^{2+} dynamics within striated muscle cell. The sarcoplasmic reticulum maintains its shape and organization despite repeated muscle cell contractions, through mechanisms which are still under investigation. The ESCRT complexes are essential to organize membrane subdomains and modify membrane topology in multiple cellular processes. Here, we report for the first time that ESCRT-II proteins play a role in the maintenance of sarcoplasmic reticulum integrity in *C. elegans*. ESCRT-II proteins colocalize with the sarcoplasmic reticulum marker ryanodine receptor UNC-68. The localization at the sarcoplasmic reticulum of ESCRT-II and UNC-68 are mutually dependent. Furthermore, the characterization of ESCRT-II mutants revealed a fragmentation of the sarcoplasmic reticulum network, associated with an alteration of Ca^{2+} dynamics. Our data provide evidence that ESCRT-II proteins are involved in sarcoplasmic reticulum shaping.

KEY WORDS: ESCRT-II, Sarcoplasmic reticulum, Organelle shape, *Caenorhabditis elegans*

INTRODUCTION

The sarcoplasmic reticulum is an endomembrane network that regulates Ca^{2+} dynamics and controls the excitation–contraction coupling in striated muscle cells. Sarcoplasmic reticulum comprises cisternae and tubular sections that are specifically responsible for the liberation and reuptake of Ca^{2+}, respectively, and is tightly linked to both the sarcomere contractile unit and sarcolemma. Recent data show that sarcoplasmic reticulum is maintained close to the myofibrils, thanks to molecular links made of the sarcomeric giant protein obscurin, the ankyrin sAnk1.5 and the tropomodulin Tmod3 (Bagnato et al., 2003; Lange et al., 2009; Ackermann et al., 2011; Gokhin and Fowler, 2011). The shape of the sarcoplasmic reticulum is also modified in the absence of the ryanodine receptor (RyR) (Maryon et al., 1998), and a recent work suggests that Trisk95, a Triadin isoform, participates in the organization of the sarcoplasmic reticulum (Fourest-Lieuvin et al., 2012). Additionally, alteration of the phosphoinositide phosphatase myotubularin MTM1, which leads to human centronuclear myopathies, results in sarcoplasmic reticulum remodeling and disorganization of the contact zone between sarcoplasmic reticulum and sarcolemma (Amoasii et al., 2013).

In eukaryotes, the endosomal sorting complexes required for transport (ESCRT-0 to ESCRT-III) were initially identified as key proteins involved in the sorting of ubiquitylated membrane proteins into intraluminal vesicles during multivesicular bodies maturation (Hanson and Cashikar, 2012; McCullough et al., 2013). ESCRT proteins display additional key cellular functions in membrane remodeling during exosome biogenesis (Colombo et al., 2013), enveloped virus budding (Garrus et al., 2001; Carlton and Martin-Serrano, 2007), cell cytokinesis membrane abscission (McCullough et al., 2013), immunological synapse formation (Choudhuri et al., 2014), plasma membrane repair (Jimenez et al., 2014) and in the biogenesis of the nuclear membrane (Webster et al., 2014; Olmos et al., 2015; Vietri et al., 2015). Interestingly, ESCRT-II, a heterotetramer complex comprising VPS-22/EAP30, VPS-36/EAP45 and two VPS-25/EAP20 subunits, has also been associated with regulation of gene expression (Irion and St Johnston, 2007; Kamura et al., 2001; Jin et al., 2005). Studies of the ESCRT functions during *Caenorhabditis elegans* development indicate that ESCRT mutant phenotypes are heterogeneous. It is noteworthy that ESCRT proteins are required early during *C. elegans* embryogenesis (Roudier et al., 2005; Michelet et al., 2009), albeit ESCRT-II mutants have late developmental defects (Djeddi et al., 2012). This observation supports a hypothesis of a different role for ESCRT-II components compared to that of other ESCRTs in *C. elegans*. Here, we used a combination of imaging and genetic techniques to test the cellular function of ESCRT-II in *C. elegans*. We present the first direct evidence that ESCRT-II, but not ESCRT-0, ESCRT-I and ESCRT-III complexes, localize to the sarcoplasmic reticulum, and that ESCRT-II and UNC-68/RyR localization at the sarcoplasmic reticulum are mutually dependent. We also show that the depletion of ESCRT-II components results in alterations of sarcoplasmic reticulum shape, Ca^{2+} dynamics and muscular contraction. Overall, this study indicates that ESCRT-II contributes to the maintenance of the sarcoplasmic reticulum architecture and function.

RESULTS

ESCRT-II proteins localize to muscle sarcomeres

C. elegans ESCRT mutants have heterogeneous phenotypes, which could be explained by the functional pleiotropy of ESCRT genes. However, ESCRT-II mutants display a rather homogenous phenotype with late developmental defects (Djeddi et al., 2012), suggesting a particular role for ESCRT-II components in this organism. To further investigate *C. elegans* ESCRT-II function, we analyzed the localization of the ESCRT-II proteins VPS-22, VPS-25 and VPS-36. We generated GFP-tagged transgenic strains (Fig. 1A), which could rescue the corresponding null mutants

[1]Institute for Integrative Biology of the Cell (I2BC), CEA, CNRS, Univ. Paris-Sud, Université Paris-Saclay, Gif-sur-Yvette cedex 91198, France. [2]Brigham and Women's Hospital, 1 Jimmy Fund Way, Boston, MA 02115, USA. [3]Faculté de médecine Paris Descartes, Inserm U1001 - 24, rue du Faubourg St-Jacques, Paris 75014, France.
*These authors contributed equally to this work

‡Authors for correspondence (renaud.legouis@i2bc.paris-saclay.fr; emmanuel.culetto@i2bc.paris-saclay.fr)

Received 6 August 2015; Accepted 15 February 2016

Journal of Cell Science (2016) 129, 1490-1499 doi:10.1242/jcs.178467

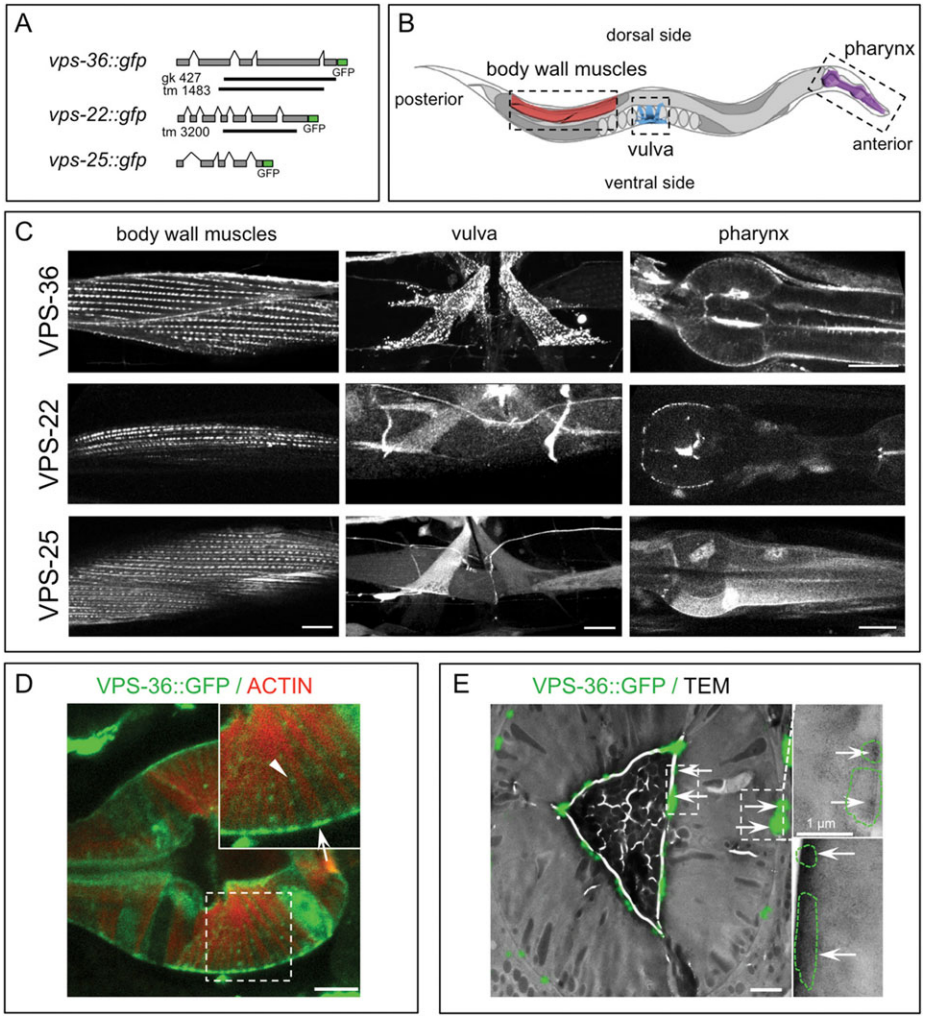

Fig. 1. Localization of ESCRT-II proteins in *C. elegans* muscle cells. (A) Schematic representation of the genomic organization of *vps-36*, *vps-22* and *vps-25* genes. Green rectangles indicate the GFP tag, and black bars indicate deletions in *vps-36* and *vps-22* mutant alleles. (B) Schematic representation of *C. elegans* showing the localization of muscle cells expressing ESCRT-II GFP-tagged proteins. Only a small section of BWM areas is shown. (C) *In vivo* confocal images of VPS-36::GFP, VPS-22::GFP and VPS-25::GFP proteins in the BWM cells, the vulva muscle cells and the terminal bulb of the pharynx of young adult animals. Scale bars: 10 µm. (D) Confocal image of VPS-36::GFP (green) and actin (red) in pharyngeal myoepithelial cells of the terminal bulb. VPS-36 is localized at actin fiber sites of attachment on basal (arrow) and apical sides, and in puncta (arrowhead) between actin filaments. Inset, a two-fold magnification. Scale bar: 5 µm. (E) CLEM analysis of VPS-36::GFP in pharyngeal muscle cells. Left image is the merge of GFP signal (green) and electronic micrograph (transversal section of the pharynx at the level of the isthmus) showing that VPS-36 is mainly associated with the apical and basal membranes (arrows). Insets are higher magnifications of the areas marked by dotted white rectangles. Green dotted lines indicate the zone of GFP signal. Scale bar: 2 µm (main image).

(Fig. S1A–C). Contrary to previously characterized ESCRT proteins (Roudier et al., 2005; Michelet et al., 2009; Djeddi et al., 2012), the ESCRT-II components were enriched in pharyngeal, vulval and body wall muscles (BWM), and were globally detected in punctate structures (Fig. 1B,C). In BWM cells, ESCRT-II puncta were regularly aligned in parallel lines along the main axis of the cells (Fig. 1C). In vulval muscles, the ESCRT-II puncta were both cortical and cytoplasmic, but VPS-22::GFP expression was weaker and VPS-25::GFP was more diffuse. In pharyngeal muscles, ESCRT-II puncta localized at the sites of attachment of actin cables (Fig. 1D,E; Fig. S1D), similar to the localization of the actin attachment protein paxillin/PXL-1 (Warner et al., 2011). We thereafter focused our study on BWMs, which are functionally and structurally similar to mammalian striated muscle (Waterston, 1988; Benian and Epstein, 2011).

ESCRT-II localizes at the sarcoplasmic reticulum attachment zones

The sub-cellular localization of ESCRT-II in BWMs was investigated by performing co-localization experiments with muscle cell markers, namely ATN-1/α-actinin, DEB-1/vinculin and actin (Fig. 2A–C; Fig. S2A,B). VPS-36::GFP shows two sites of localization in the sarcomere. The majority of the signal largely co-localized with ATN-1/α-actinin (Fig. 2B; Fig. S2A) or DEB-1/vinculin (Fig. S2B), suggesting that it is strongly associated with dense bodies (Fig. 2A), the actin attachment structures corresponding to both vertebrates Z discs and costameres. However, VPS-36::GFP was also present in small patches localized between aligned dense bodies, probably apposed to the sarcolemma (arrows in Fig. 2B; Fig. S2B). Correlative light-electron microscopy (CLEM) on BWMs confirmed that VPS-36 was associated with both dense bodies and an electron-dense structure that was localized between the plasma membrane and the lattice of contractile filaments (Fig. 2C). This pattern corresponds to the organization of the sarcoplasmic reticulum network within BWMs (Fig. 2A), which forms thin tubular structures along the dense bodies and the plasma membrane (Hammarlund et al., 2000). A similar localization to that of VPS-36 was also detected for the ESCRT-II subunits VPS-25::GFP and VPS-22::GFP (Fig. S2B). The localization of endogenous ESCRT-II was further confirmed using two antibodies directed against VPS-36 (this study) and the whole ESCRT-II complex (Schuh et al., 2015), respectively (Figs 2B and 3). Moreover, the co-localization analysis with the RyR UNC-68, involved in sarcoplasmic reticulum Ca^{2+} release, indicated that ESCRT-II localized to the sarcoplasmic reticulum (Fig. 2B). To further support the link between sarcoplasmic reticulum and ESCRT-II proteins, we analyzed the localization of ESCRT-II in the *unc-68(e540)* mutant, which exhibits an alteration of the sarcoplasmic reticulum (Maryon et al., 1998; Cho et al., 2000). In *unc-68*

Journal of Cell Science (2016) 129, 1490-1499 doi:10.1242/jcs.178467

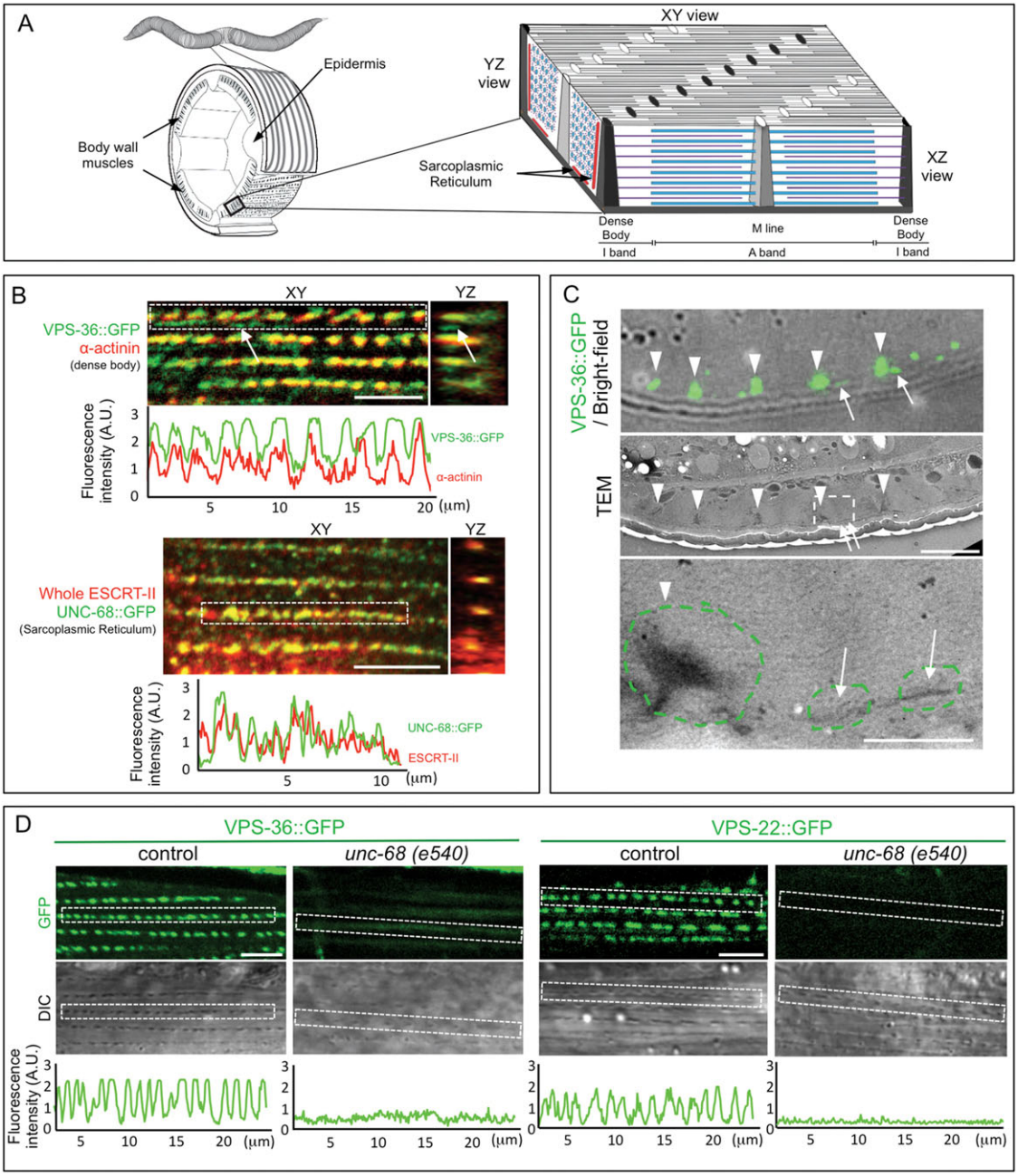

Fig. 2. The localization of ESCRT-II in muscles corresponds to the sarcoplasmic reticulum network. (A) Schematic representation of *xy*, *yz* and *xz* cross-sections of ventral *C. elegans* BWM cells showing the actin (purple) and myosin (blue) filaments, the contractile filaments anchoring dense body structures (black) and M-lines (gray). The BWM cell sarcolemma is in dark gray, and the sarcoplasmic reticulum is shown as red tubules. (B) Merged images of single confocal sections of BWM (*xy* and *yz* views) from transgenic strains expressing (upper panel) VPS-36::GFP [and stained with antibodies directed against GFP (green) and dense body marker α-actinin (red)] or (lower panel) the sarcoplasmic reticulum marker UNC-68::GFP [and stained with antibodies directed against GFP (green) and the whole ESCRT-II (red)]. White arrows point to VPS-36::GFP signal localized between dense bodies and the bottom of the sarcolemma (*yz* view of the muscle sarcolemma that faces the hypodermis is on the left). Scale bar: 5 µm. Graphs represent the fluorescence intensity of green and red signals measured in the corresponding dotted rectangle. (C) Correlative light (upper panel) and electron microscopy (middle panel) analysis of VPS-36::GFP from a transversal section of BWM. 80% of dense bodies (arrowheads, *n*=237) and 50% of electron-dense structures that were localized next to the muscle cell plasma membrane (arrows, *n*=162) were positive for the VPS-36::GFP signal. Scale bar: 5 µm. Lower panel is a higher magnification of the area marked with a dotted rectangle. Scale bar: 1 µm. (D) Single confocal and DIC images of BWM cells expressing VPS-36::GFP or VPS-22::GFP from either control or *unc-68* mutant animals. The DIC shows the rows of dense bodies. The graph represents the fluorescence intensity measured in the dotted rectangle. Scale bar: 5 µm.

animals, the subcellular localization of both VPS-36 and VPS-22 was strongly decreased in BWMs (Fig. 2D), albeit unaffected in pharyngeal and vulval muscles (Fig. S2C). This data shows that the localization of ESCRT-II subunits at the sarcoplasmic reticulum is dependent on UNC-68.

To analyze whether the localization to sarcoplasmic reticulum is specific for ESCRT-II complex, we then performed immunostaining using antibodies directed against VPS-27 (ESCRT-0), VPS-23 (ESCRT-I), VPS-20 and VPS-32 (ESCRT-III) (Fig. 3; Fig. S2D). We observed that neither VPS-27, nor VPS-

Journal of Cell Science (2016) 129, 1490-1499 doi:10.1242/jcs.178467

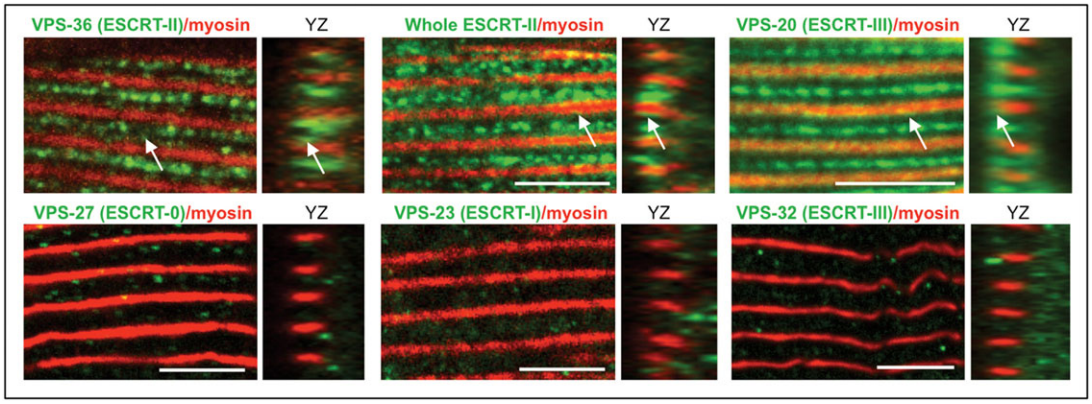

Fig. 3. The localization at the sarcoplasmic reticulum is specific for ESCRT-II subunits and VPS-20. Confocal images (*xy* and *yz* views) of fixed BWM cells from wild-type worms stained for both myosin (red) and endogenous ESCRT subunits (green): ESCRT-0, VPS-27; ESCRT-I, VPS-23; ESCRT-II, VPS-36; the whole ESCRT-II complex; ESCRT-III, VPS-20 and VPS-32. Antibodies recognizing VPS-36, whole ESCRT-II complex and VPS-20 showed the similar specific staining within the I band and at the interface between A and I bands (arrows), whereas other ESCRT subunits were not or were barely detected at these subcellular localizations. Scale bar: 5 µm.

23 or VPS-32 localized in muscle cells, similar to ESCRT-II subunits. However, VPS-20 (ESCRT-III), which directly interacts with ESCRT-II (Schuh et al., 2015), was also detected at the sarcoplasmic reticulum. These observations indicate that the localization to the sarcoplasmic reticulum is not a common characteristic of all ESCRT components, but specific for ESCRT-II and VPS-20.

The structure of the sarcoplasmic reticulum network is altered in ESCRT-II mutants

To decipher the function of ESCRT-II proteins on sarcoplasmic reticulum, we performed transmission electron microscopy (TEM) and analyzed the subcellular structure of BWM cells in *vps-36 (tm1483)* and *vps-22(tm3200)* mutants. In both mutants, the sarcomeric contractile apparatus is only slightly affected, with few misaligned filaments (Fig. S3A). These data confirmed our previous observation that myosin and actin staining appears normal in mutant worms, and indicate that mutations in ESCRT-II do not profoundly alter the ultrastructure of BWM cell contractile filaments.

However, we observed defects in the structure of the sarcoplasmic reticulum in *vps-36(tm1483)* and *vps-22(tm3200)* BWMs. TEM pictures revealed that the sarcoplasmic reticulum was significantly fragmented, whereas the size of the dense bodies was unaffected (Fig. 4A; Fig. S3). Quantitative analysis of TEM pictures showed that, in *vps-36* and to a lesser extent in *vps-22* mutants, the size of sarcoplasmic reticulum tubules parallel to dense bodies was decreased, but their number was higher compared to that in wild-type animals (Fig. 4B,C). The sarcoplasmic reticulum that was associated with sarcolemma was also fragmented in *vps-36* animals (Fig. S3E,F).

To support the TEM-based observations, we then analyzed in ESCRT-II mutants two well-characterized sarcoplasmic reticulum components – UNC-68/RyR and SCA-1/SERCA, a Ca^{2+}ATPase pump required to refill sarcoplasmic reticulum. In BWM sarcomeres, the localization of both SCA-1 and UNC-68 was similar to that of the ESCRT-II proteins (Fig. 5A,B). No strong modification of the localization of SCA-1 was detected in *vps-36* mutants (Fig. 5A), confirming that a sarcoplasmic reticulum network was still present in *vps-36* BWMs. However, the localization of UNC-68/RyR protein was affected in both *vps-36 (gk427)* and *vps-22(tm3200)* mutants (Fig. 5B). UNC-68::GFP expression was reduced in the muscle cell, and almost no signal could be observed in the sarcomere.

Together with the TEM analysis, our data indicate that the sarcoplasmic reticulum network is present in ESCRT-II mutants but shows characteristic alterations. Moreover, these experiments indicate that UNC-68/RyR and ESCRT-II are involved in the correct localization of each other in a reciprocal manner at sarcoplasmic reticulum.

ESCRT-II mutants have defects in Ca^{2+} dynamics and locomotion behavior

We used the Ca^{2+} bio-sensor indicator GCaMP3.35 to analyze the Ca^{2+} dynamics in BWMs of *vps-36* animals (Schwarz et al., 2012). Time-lapse analyses and quantifications revealed that the intensity of GCaMP3.35 was globally reduced in *vps-36* mutants (Fig. 5C,D; Movies 1 and 2). However, the intensity of GCaMP3.35 could locally reach levels similar to those in the control, suggesting that BWMs are still able to produce Ca^{2+} transients, but less efficiently. These results demonstrate that ESCRT-II is essential for the integrity of Ca^{2+} homeostasis in muscle cells. We then asked whether the sarcoplasmic reticulum structure and muscle Ca^{2+} dynamic defects of ESCRT-II mutants result in a modification of the muscle physiology. We therefore analyzed pharyngeal contractions and locomotion of *vps-36 (tm1483)*, *vps-36(gk427)* and *vps-22(tm3200)* animals (Fig. 6). Macroscopic observation of *vps-36* and *vps-22* animals revealed pharyngeal pumping and locomotion defects (Fig. 6A) (data not shown) only during late larval development. To further study and quantify the locomotion defect, we performed an electrotaxis analysis (Manière et al., 2011) to check that *vps-22* and *vps-36* heterozygous animals had wild-type locomotion (Fig. 6B). The speed locomotion of synchronized populations of heterozygous and homozygous *vps-22(tm3200)* and *vps-36(tm1483)* animals was then analyzed during larval development. From the third larval stage, we observed a decreased velocity of both *vps-22* and *vps-36* mutants compared to that of the controls (Fig. 6C). Additionally, the locomotion defect further increased during development. To check that the locomotion defect of ESCRT-II mutants was due to the function of ESCRT-II in BWMs, muscle-specific RNA interference (RNAi) (Kashyap et al., 2012) was performed against *vps-36*, *vps-22* and *vps-32*. *vps-36 (muscleRNAi)*, *vps-22(muscleRNAi)* but not *vps-32(muscleRNAi)*

Journal of Cell Science (2016) 129, 1490-1499 doi:10.1242/jcs.178467

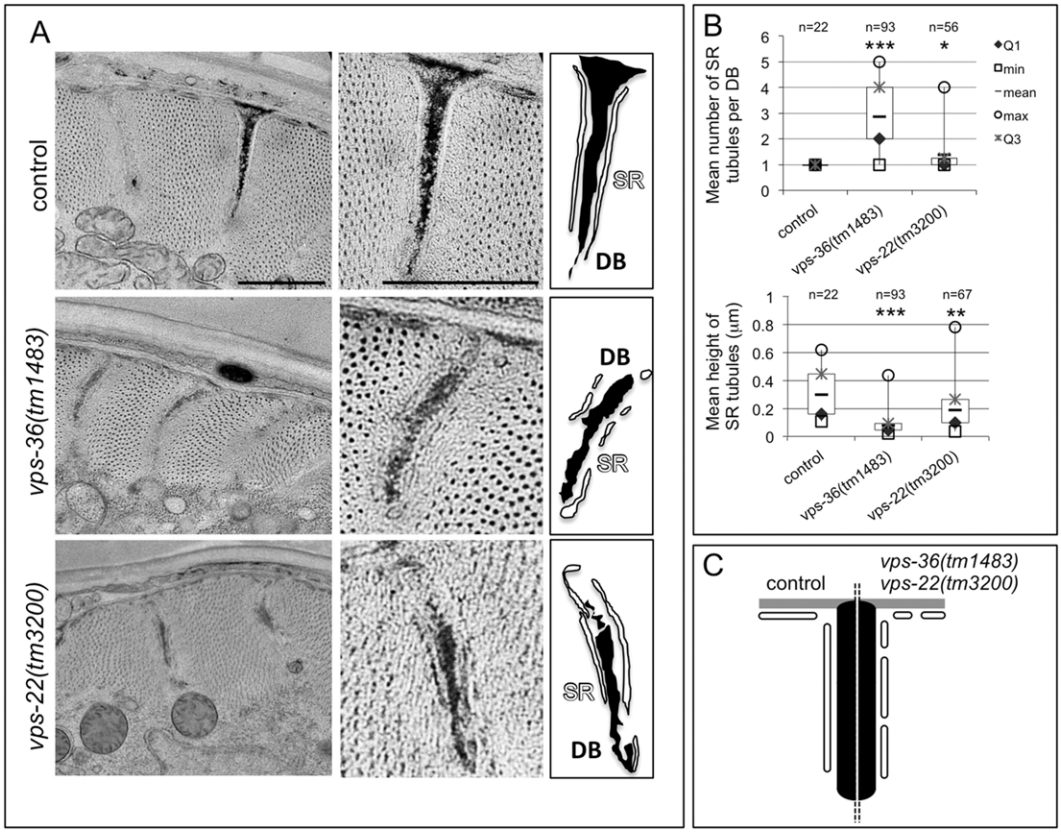

Fig. 4. The structure of the sarcoplasmic reticulum network is altered in *vps-36* and *vps-22* mutants. (A) TEM analysis of transverse sections of control, *vps-36(tm1483)* and *vps-22(tm3200)* animals (left panels). Middle and right panels show a higher-magnification image of one dense body with surrounding sarcoplasmic reticulum (SR) and their corresponding schematics, respectively. Images are representative of the analyses of at least 12 dense bodies (DB). Scale bar: 1 µm. (B) Quantification of the number of sarcoplasmic reticulum tubules associated to the dense bodies (upper panel) and the mean height of the sarcoplasmic reticulum tubules (lower panel) in control, *vps-36* and *vps-22* animals. *n* indicates the number of measurements, based on 12 to 29 dense bodies from two or three animals. Boxplots illustrate the measure distribution as indicated. *, ** and *** indicate a statistically significant difference between mutant and control animals by a Mann–Whitney-Wilcoxon test with $P<0.01$, $P<0.001$ and $P<0.0001$, respectively. (C) Schematic representation of the sarcoplasmic reticulum defect in *vps-36* and *vps-22* mutants compared to control animals.

animals displayed a reduced velocity compared to the controls (Fig. 6D). This result indicates that ESCRT-II mutants show a reduction of locomotion behavior, which correlates with the sarcoplasmic reticulum ultrastructural and Ca^{2+} dynamic defects observed in muscle cells.

DISCUSSION

Altogether, the data in our study describe a previously unidentified function for ESCRT-II components in controlling the maintenance of sarcoplasmic reticulum shape. We present here the first direct evidence that ESCRT-II components VPS-36, VPS-22 and VPS-25 share a specific sarcoplasmic reticulum sub-cellular localization in *C. elegans* muscle cells. The lack of colocalization with ESCRT subunits other than VPS-20 suggests a role that is not linked to endosome maturation. Interestingly, a genomic screen performed in *Drosophila*, indicates that muscle-specific knockdown of *Vps25* and *Vps36* genes are lethal at the late pupal and pharate stages, respectively, supporting that both genes are involved in muscle morphogenesis and function in *Drosophila* (Schnorrer et al., 2010). These data suggest that ESCRT-II function in muscle cells could be evolutionarily conserved between *Drosophila* and *C. elegans*. Vaccari et al. (2009) have obtained *Drosophila melanogaster* null mutants for most of the genes encoding the four ESCRT complexes. They show that *vps22*- and *vps25*-mutant germline cells frequently lack subcortical actin skeleton, with alterations of the plasma membrane integrity. These data suggest that ESCRT-II could be involved in maintaining membrane integrity.

Several clues from the literature could explain how ESCRT-II is recruited to the sarcoplasmic reticulum membrane. The ESCRT-II complex contains several protein–protein-interaction and phosphoinositide-binding domains that could mediate its localization to the sarcoplasmic reticulum membrane. The predicted N-terminal helix structure (H0) of VPS-22 participates in membrane binding, together with the VPS-36 GLUE domain (Im and Hurley, 2008). Importantly, both domains mediate the binding of the whole ESCRT-II complex to phosphatidylinositol 3,5-bisphosphate and phosphatidylinositol (3,4,5)-trisphosphate phosphoinositide membranes, and therefore could be involved in the localization of ESCRT-II at sarcoplasmic reticulum membranes, where tight regulation of phosphoinositide content could have a key structural role (Amoasii et al., 2013). The VPS-20 ESCRT-III subunit is able to bind to ESCRT-II (Fyfe et al., 2011) in a curvature-dependent manner, and VPS-20 decreases the ESCRT-II affinity for flat lipid bilayers. It is therefore possible that ESCRT-II and ESCRT-II associated with VPS-20 could be localized to flat and curved sarcoplasmic reticulum membrane, respectively. Interestingly, the ESCRT subunit CHMP7 has been recently shown to be involved in endoplasmic reticulum dynamics in yeast (Bauer et al., 2015) and during the process of nuclear envelop reformation in metazoans (Vietri et al., 2015). Noticeably,

Journal of Cell Science (2016) 129, 1490-1499 doi:10.1242/jcs.178467

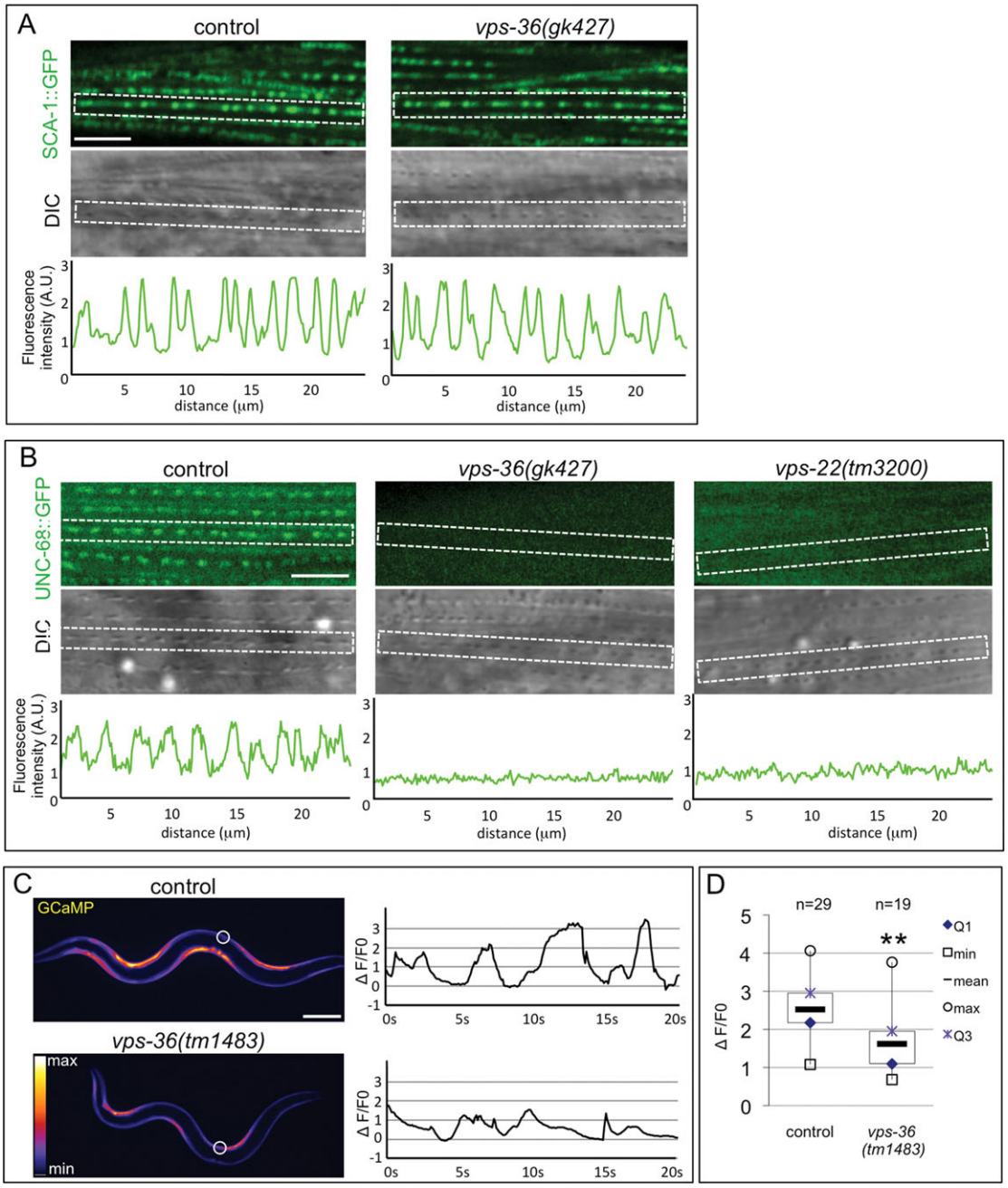

Fig. 5. UNC-68 localization to the sarcoplasmic reticulum and Ca^{2+} dynamics are altered in *vps-36* mutant. (A) Confocal image (upper panel) and the corresponding DIC picture (lower panel) of *vps-36* mutants expressing SCA-1::GFP. Graphs represent the fluorescence intensity measured in the dotted rectangle. Scale bar: 5 µm. (B) Confocal image (upper panel) and the corresponding DIC picture (lower panel) of control, *vps-36* and *vps-22* mutants expressing UNC-68::GFP. Graphs represent the fluorescence intensity measured in the dotted rectangle. Scale bar: 5 µm. (C) *In vivo* analysis of transgenic worms expressing the GCaMP3.35 Ca^{2+} biosensor indicator in BWM cells. Representative images and fluorescence records plotted as ΔF/F0 for the indicated region of interest (white circle) of control and *vps-36* mutant animals expressing GCaMP3.35. The bright signal in BWM cells indicates the Ca^{2+} intensities. Scale bar: 100 µm. (D) Boxplots of ΔF/F0 peak values associated with muscle contractions obtained from control and *vps-36* animals during the 20 s acquisition time. *n* values represent the number of peaks. ** indicates a statistically significant difference between mutant and control animals by a Mann–Whitney-Wilcoxon test (*P*<0.001).

CHMP7 appears to be an in-frame fusion between VPS20-like and VPS25-like domains.

In vitro studies have shown that ESCRT-II together with ESCRT-I can induce deformation of the membrane surface of giant unilamellar vesicles, and one can imagine a similar function for ESCRT-II at the level of the sarcoplasmic reticulum. By analogy with the known functions of ESCRT in regulating membrane topology, three molecular mechanisms could explain how ESCRT-II controls sarcoplasmic reticulum shape. Firstly, VPS-22 has a cationic amphipathic helix that can insert into a membrane and modify its curvature (Im and Hurley, 2008). Secondly, *in vitro* studies have shown that ESCRT-II can assemble to form clusters of 10–100 molecules on a lipid bilayer and induce a lipid-phase separation, which could modify the membrane and lead to fragmentation (Boura et al., 2012). Thirdly, the partially curved shape of ESCRT-II and its high capacity for membrane interactions

Journal of Cell Science (2016) 129, 1490-1499 doi:10.1242/jcs.178467

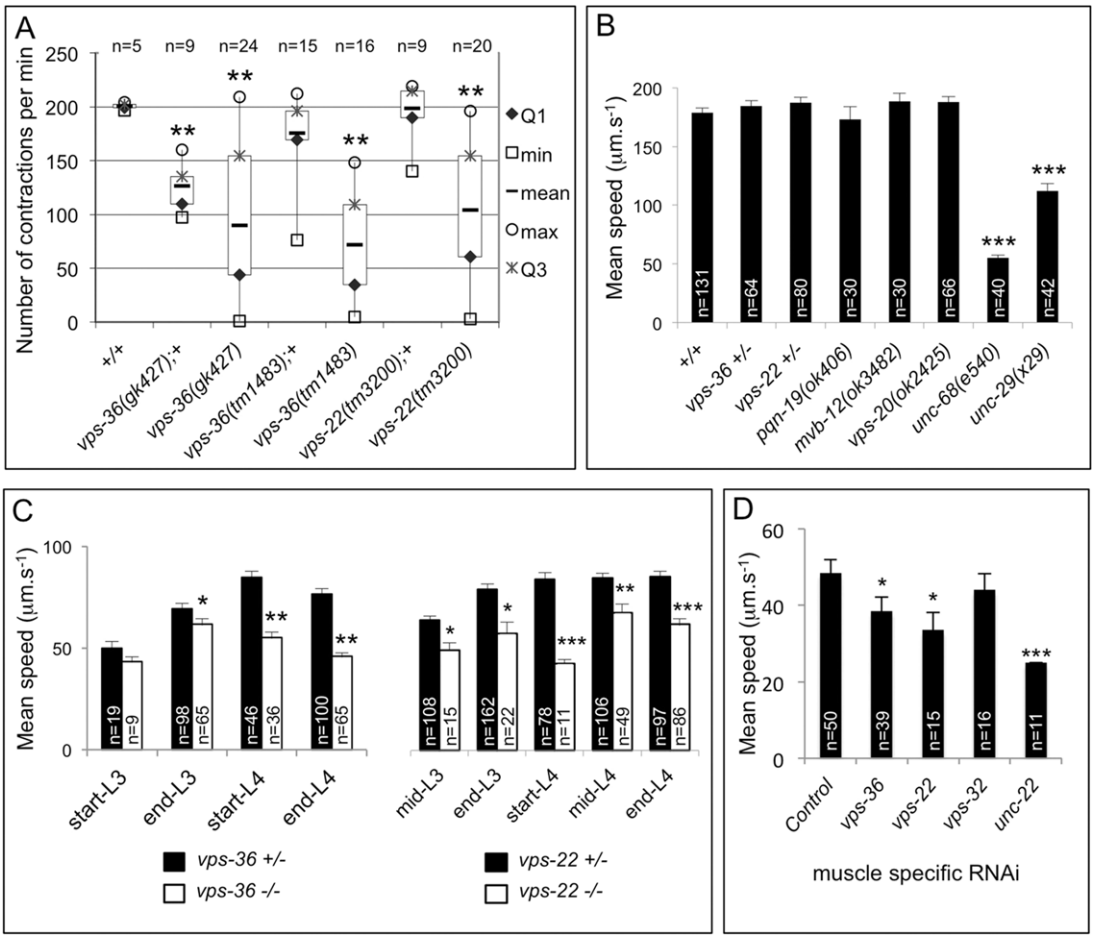

Fig. 6. ESCRT-II mutants present defects in pharyngeal contraction and locomotion. (A) Boxplots of pharyngeal contraction number per minute in control and ESCRT-II mutants, *n* is the number of young L4 larvae analyzed. ** indicates a statistically significant difference between mutant and control animals by a Mann–Whitney-Wilcoxon test (P<0.01). (B) The mean speed of locomotion in µm s^{-1} was determined for heterozygote *vps-36* and *vps-22* mutants, viable homozygous *pqn-19* (ESCRT-0), *mvb-12* (ESCRT-I), *vps-20* (ESCRT-III) and locomotion-deficient *unc-68* and *unc-29* mutants. Error bars are s.e.m., *n* is the number of animals. *** indicates a statistically significant difference between mutant and wild-type animals calculated using a Welch's *t*-test (P<0.001). (C) Electrotaxis was performed on a mixed population of heterozygous (control animals) and homozygous *vps-36(gk427)* or *vps-22(tm3200)* mutant animals between the third and fourth larval stages (L3 and L4, respectively). The mean speed of locomotion in µm s^{-1} was determined. Error bars are s.e.m., *n* is the number of animals.*, ** and *** indicate a statistically significant difference between heterozygous and homozygous mutants calculated using an unpaired Student's *t*-test (P<0.05, P<0.01 and P<0.001, respectively). (D) Mean speed of locomotion of muscle-specific RNAi mutants. * and *** indicate a statistically significant difference between control and RNAi animals calculated using an unpaired Student's *t*-test (P=0.05 and P<0.01, respectively).

could mean that it acts as a scaffold for the sarcoplasmic reticulum membrane curvature (Mercker and Marciniak-Czochra, 2015). Depletion of ESCRT-II from the sarcoplasmic reticulum would affect membrane topology and lead to defective maintenance of the sarcoplasmic reticulum. Further studies will be necessary to identify the precise function of the ESCRT-II complex in relation to other proteins involved in sarcoplasmic reticulum shaping.

MATERIALS AND METHODS

C. elegans strains

General methods for the maintenance of *C. elegans* have been described previously (Brenner, 1974). Worms were cultured on nematode growth medium (NGM) agar plates, plated with *Escherichia coli* OP50 strain, at 20°C unless otherwise indicated. We used the N2 (Bristol) wild-type strain. The following mutant alleles and transgenic markers were used: HT1593 *unc-119(ed3)III*; CB2065 *dpy-11(e224)unc-76(e911)V*; VC947 *vps-36 (gk427)V/nT1 [qIs51](IV;V)*; TM1483 *vps-36(tm1483)V*; TM3200 *vps-22 (tm3200)III*; CB540 *unc-68(e540)V*; DM7335 *pxl-1(ok1483)III; raEx335 [pxl-1a::GFP; rol-6(su1086)], sca-1::gfp* (gift from K.R. Norman), HK205 *khIs22[unc-68::GFP; rol-6(su1086)]*; RB1875 *vps-20(ok2425)*I; RB2514 *mvb-12(ok3482)IV*; RB674 *pqn-19(ok406)I*; *unc-29(x29)* (gift from Jean-Louis Bessereau, Université Claude Bernard Lyon1, CGphiMC, Lyon, France). The mutant strain RD116 *vps-36(gk427)V/dpy-11(e224)unc-76 (e911)V* was obtained by crossing VC947 with CB2065. The mutant strain RD117 was obtained by crossing TM1483 with CB2065. The mutant strain RD139 *vps-22 (tm3200)*III/*unc-119(ed3)III* was obtained by crossing TM3200 (Shohei Mitani, National BioResource Project) with HT1593. RD116, RD117 and RD139 were outcrossed four to six times to N2 before any phenotype analysis. RD323 *vps-36(gk427)V;goeIs3[pmyo-3::GCamP3.35::unc-54–3′utr;unc-119(+)]V* was obtained by crossing RD116 with HBR4 *goeIs3[pmyo-3::GCamP3.35::unc-54–3′utr; unc-119 (+)]V*.

Transgenesis

The transgenes *Pvps-22::vps-22::gfp*, *Pvps-25::vps-25::gfp* and *Pvps-36::vps-36::gfp* were constructed using a PCR-based protocol (Hobert, 2002). *C. elegans* transgenic strains RD163: *ppEx163[Pvps-22::vps-22::gfp; rol-6 (su1006)]*, RD112: *ppEx112[Pvps-36::vps-36::gfp; rol-6(su1006)]* and RD324 *ppEx324[Pvps-25::vps-25::gfp; rol-6(su1006)]* were obtained by microinjection of the PCR products of interest associated with a plasmid expressing the *rol-6(su1006)* phenotypic markers (Mello and Fire, 1995). F1

[Rol] animals from injected animals were selected and isolated to generate independent transgenic strains. At least two independent strains were studied to verify consistency of GFP signal before any further use.

For rescue experiments, the strain RD281: *vps-22(tm3200)III; ppEx163 [Pvps-22::vps-22::gfp; rol-6(su1006)]* was obtained by crossing male heterozygote *vps-22(tm3200)*III/+ with RD163. Subsequently, F1 [GFP, Rol] hermaphrodites were isolated for egg laying. Founder animals were genotyped by performing PCR to select lines harboring the *vps-22(tm3200)* deletion allele. F2 animals from positive lines were subsequently individualized for egg laying then genotyped by performing PCR to select homozygous mutants with [GFP, Rol] phenotypes. A similar procedure was performed to test *vps-36* mutant rescue. RD283: *vps-36 (tm1483)V; ppEx112[Pvps-36::vps-36::gfp; rol-6(su1006)]* and RD242: *vps-36 (gk427)V; ppEx112[Pvps-36::vps-36::gfp; rol-6(su1006)]*.

Muscle-specific RNAi

We used the transgenic strain ALF110: *rde-1(ne219); bafIs110[Pmyo-3::rde-1; Pmyo-3::GFP]* to specifically inactivate ESCRT genes that were expressed in body wall muscle cell (Kashyap et al., 2012) using the feeding RNAi technique with a previously described protocol (Djeddi et al., 2012). L4 larvae-stage animals were cultivated on RNAi plates at 20°C that had been seeded with bacteria clones (Ahringer RNAi library, except *vps-36* from Open Biosystems) expressing dsRNA against *vps-36*, *vps-22* and *vps-32*. Bacteria clones HT115 with either the empty vector L4440 or expressing dsRNA against *unc-22* were used as negative and positive controls, respectively. When worms reached the adult stage and started to lay eggs, they were transferred to new plates three times a day. F1 progeny were subsequently analyzed for locomotion phenotype defects when they reached the one-day adult stage using the electrotaxis method.

Electron microscopy

L4 stage N2, *vps-36(tm1483)* and *vps-22(tm3200)* animals were transferred into M9 buffer with 20% BSA to 200-µm-deep flat carriers, followed by freezing in the EMPACT-2 HPF apparatus (Leica Microsystems) and cryo-substitution with acetone as described previously (Kolotuev et al., 2010). Blocks were further infiltrated with 100% EPON and then embedded in fresh EPON. Ultrathin sections of 80 nm were cut on an ultramicrotome, and were collected on formvar- and carbon-coated copper grid. Sections were contrasted with 2% uranyl acetate for 15 min and 0.08 M lead citrate for 8 min. Sections were observed with a Jeol 1400 TEM instrument at 120 kV, and images were acquired with a Gatan 11 Mpixels SC1000 Orius CCD camera.

For correlative microscopy, samples were frozen with an EMPACT2 instrument (Leica) and prepared as described previously (Watanabe et al., 2012). Cryosubstitution was performed at −90°C in 0.01% osmium in 95% acetone-5% water. Sample dehydration was performed in 0.1% uranyl acetate in 95% acetone-5% water. Solvent was exchanged for glycol methacrylate resin (30, 70 and then 100%) in 95% ethanol with 5% water at −30°C. Resin polymerization was performed at −30°C with N,N-dimethyl-p-toluidine. Thin sections of 200 nm were cut and collected on 200 mesh copper finder. Photonic images were acquired with an epifluorescence microscope (Zeiss) equipped with an EMCCD camera.

Behavioral analyses

Electrotaxis was performed according to Manière et al. (2011) with some modifications to facilitate L3 and L4 larvae sorting. The pre-running gel solution was 2% agar, 0.25 mM NaCl. The running buffer was 0.25 mM NaCl 0.36% glycerol. The running gel was made by mixing 37.5 ml of warm pre-running gel solution (55°C) with 12.5 ml of running buffer. Worms were transferred onto a NGM plate without bacteria and washed twice in running buffer and then deposited onto the running gel in a minimum liquid droplet. The worms were run for 8 min at 230 V 20 mA. Then the gel was removed and cut transversally into four slices, which represent 2 cm, 3 cm, 4 cm and 5 cm distances from the start point. Strips of gel were transferred to large OP50 NGM plates for counting and phenotyping of worms.

To monitor pharyngeal function, synchronized N2, RD116, RD117 and RD139 worms were individualized at the start of L4 stage on NGM OP50 plates. Worms were acclimated to the plates for 5 min at room temperature (20 to 23°C) and the number of pharyngeal contractions was counted under the dissecting microscope.

Immunolocalization

The NH_2 terminal 18-amino-acid long polypeptide from VPS-36 was synthetized (Neosystem) and used to immunize two rabbits. Final immunosera were purified on an affinity chromatography column (immunobilization Kit 2, Pierce).

Immunolocalization was performed as previously described (Manil-Ségalen et al., 2014). Worms were collected and resuspended in 4 ml of fixative solution [0.25 ml 16% formaldehyde; 2.85 ml 100% methanol, 1 ml 4× fixation buffer (320 mM KCl, 80 mM NaCl, 40 mM EGTA, 60 mM PIPES pH 7.4, 20 mM spermidine)], immersed in liquid nitrogen for 2 min, then fixed at 4°C for 2 h. Worms were washed three times in 1 ml of TTB buffer (100 mM Tris-HCl pH 7.4, 1% Triton X100, 1 mM EDTA) and incubated in 1 ml TTB 1% β-mercaptoethanol for 2 h at 37°C. Worms were washed three times in 1× BO_3 buffer (20 mM H_3BO_3, 10 mm NaOH pH 9.2) then incubated in 1 ml 1× BO_3 10% 0.1 M DTT for 15 min. After three washes in 1 ml 1× BO_3, worms were incubated in 1 ml 1× BO_3 buffer supplemented with 75 µl 30% H_2O_2 for 15 min. After two washes in 1× BO_3 buffer, worms were incubated for 20 min in 1 ml AbB (1× PBS pH 7.4, 0.1% BSA, 0.5% Triton X-100, 1 mM EDTA), washed in 1 ml AbA (1× PBS pH 7.4, 1% BSA, 0.5% Triton X-100, 1 mM EDTA) and incubated with primary antibodies against the following proteins: ATN-1/α-actinin, 1/200 (MH35, a kind gift from Kathrin Gieseler, Université Claude Bernard Lyon1, CGphiMC, Lyon, France); DEB-1/vinculin, 1/25 [MH24, Developmental Studies Hybridoma Bank (DSHB), University of Iowa, IA]; Myo-3/Myosin, 1/100 (5-6, DSHB); whole ESCRT-II (1/200) and VPS-20 (1/200) (gifts from Anjon Audhya, University of Wisconsin, WI); VPS-36, 1/200 (this study); VPS-27, 1/250; VPS-23, 1/100; VPS-32, 1/1000; and GFP, 1/200 (Invitrogen). Incubation was performed overnight at 4°C with constant agitation in the dark. Worms were washed four times, incubated with the appropriate secondary antibodies conjugated with Alexa-Fluor-488 or Alexa-Fluor-568 (1/500; Molecular Probes) for 2 h at room temperature. After four washes with 1 ml of AbB, worms were mounted in DABCO medium.

For actin immunostaining, worms were fixed in 1% formaldehyde in phosphate buffer (0.1 M pH 7.4) for 2 h, permeabilized in 1 ml of frozen acetone for 2 min and washed in 1 ml of 1× PBS. Worms were then incubated with Alexa-Fluor-568–phalloidin, 1/200 (Invitrogen), for 2 h.

Routinely, fluorescent expression and phenotypic analyses were performed with an Axioskop 2 Plus microscope (Zeiss) equipped with differential interference contrast (DIC) Nomarski optics coupled to a camera (CoolSNAP, Roper Scientific). Confocal images were captured on a confocal Leica (SP8) instrument. Image analyses and quantifications were performed with ImageJ.

Ca^{2+} imaging using GCaMP

Genetic crosses were made to transfer the genetically encoded Ca^{2+} indicator GCaMP3.35 (Schwarz et al., 2011) into the *vps-36 (gk427)* background. Heterozygous males *vps-36(gk427)/+* were crossed with homozygous HBR4: *goeIs3[Pmyo-3::GCaMP3.35::unc-54-3′UTR; unc-119(+)]*. By genetic recombination, *vps-36(gk427)HBR4/vps-36(+)HBR4* worms were recovered and maintained. GCaMP signal was analyzed in *vps-36(gk427)* homozygous progeny and compared with that in heterozygous animals.

For GCaMP analysis, progeny of *vps-36(gk427)HBR4/vps-36(+)HBR4* were immobilized on a 2% agarose pad in 5 µl of M9 buffer between the slide and coverslip. Worms were imaged every 100 ms for 20 s, then removed from the pad for phenotyping. For each acquisition, the fluorescence signal for each frame was monitored in a region of interest (ROI) with ImageJ software (http://rsb.info.nih.gov/ij/). The intensity of GCaMP3.35 was analyzed in three different ROIs defined and used for each analyzed animal: one was located in the ventral muscle cell next to the vulva, one in the BWM cell in the dorsal quadrant just opposite to the previous one, and one in the head either on the ventral or the dorsal side. The fluorescence records were first plotted as fluorescence signal over time. Then, values were plotted as ΔF/F0 using Excel. F0 is an average baseline value, which is the

mean intensity of the 20 lowest fluorescence intensities recorded during the time acquisition (Kerr, 2006). The ΔF/F0 series were compared between control and *vps-36* mutant using a Mann–Whitney-Wilcoxon test.

Statistical analysis

Data visualization and statistical analyses were performed with the R software (https://www.r-project.org). Unpaired two-tailed Student's *t*-test was used to compare the means of two samples for which there were assumptions about normality and similar variances. A Shapiro-Wilk's test was used to evaluate the normal distribution of the values within each sample. Similar variances were checked with Hartley F_{max} test. When samples did not assume equal variances, a Welch's *t*-test was performed. In case the sample did not assume normality, a Mann–Whitney-Wilcoxon non-parametric rank test was performed. We did not use statistical methods to predetermine sample size. We did not use any method of randomization to select data. The investigators were not blinded to allocation during experiments and outcome assessment. Statistics source data can be obtained upon request.

Acknowledgements

The authors would like to thank M. Jospin, K. Gieseler and C. J. Merrifield for critical reading of the manuscript. We are grateful to V. Scarcelli for technical help. We also thank Shohei Mitani (National Bioresource Project for the nematode, Japan) for providing *vps-22(tm3200)* and *vps-36(tm1483)* mutant alleles, J. Audhya for giving us antibodies against the whole ESCRT-II complex and VPS-20, Maelle Jospin (Université Claude Bernard Lyon1, CGphiMC, Lyon, France) for giving us the GCaMP3.35 strain, Keneth R. Norman (Albany Medical College, NY) for sending us SCA-1::GFP; and we thank the *Caenorhabditis* Genetic Center (CGC), which is funded by the National Institutes of Health (NIH) Office of Research Infrastructure Programs [grant number P40 OD010440], for providing several reagents and strains used in this study. This work has benefited from the facilities and expertise of the Imagif Cell Biology Unit of the Gif campus (http://www.i2bc.paris-saclay.fr/), which is supported by the Conseil Général de l'Essonne. We acknowledge the France-BioImaging infrastructure, supported by the French National Research Agency 'Investments for the future' [grant number ANR-10-INSB-04-01].

Competing interests

The authors declare no competing or financial interests.

Author contributions

R.L., E.C. and C. Lefebvre designed experiments. C. Lefebvre, E.C., C. Largeau and C.F. performed *C. elegans* experiments. X. Michelet performed preliminary experiments. E.C. and X. Maniere performed electrotaxis in the I.M. laboratory. R.L., C. Lefebvre and E.C. wrote the manuscript. All authors provided detailed comments.

Funding

The Legouis group is supported by the Agence Nationale de la Recherche (project EAT) [grant number ANR-12-BSV2-018]; and the Association pour la Recherche sur le Cancer [grant number SFI20111203826].

Supplementary information

Supplementary information available online at
http://jcs.biologists.org/lookup/suppl/doi:10.1242/jcs.178467/-/DC1

References

Ackermann, M. A., Ziman, A. P., Strong, J., Zhang, Y., Hartford, A. K., Ward, C. W., Randall, W. R., Kontrogianni-Konstantopoulos, A. and Bloch, R. J. (2011). Integrity of the network sarcoplasmic reticulum in skeletal muscle requires small ankyrin 1. *J. Cell Sci.* **124**, 3619-3630.

Amoasii, L., Hnia, K., Chicanne, G., Brech, A., Cowling, B. S., Müller, M. M., Schwab, Y., Koebel, P., Ferry, A., Payrastre, B. et al. (2013). Myotubularin and PtdIns3P remodel the sarcoplasmic reticulum in muscle in vivo. *J. Cell Sci.* **126**, 1806-1819.

Bagnato, P., Barone, V., Giacomello, E., Rossi, D. and Sorrentino, V. (2003). Binding of an ankyrin-1 isoform to obscurin suggests a molecular link between the sarcoplasmic reticulum and myofibrils in striated muscles. *J. Cell Biol.* **160**, 245-253.

Bauer, I., Brune, T., Preiss, R. and Kölling, R. (2015). Evidence for a Nonendosomal Function of the Saccharomyces cerevisiae ESCRT-III-Like Protein Chm7. *Genetics* **201**, 1439-1452.

Benian, G. M. and Epstein, H. F. (2011). Caenorhabditis elegans muscle: a genetic and molecular model for protein interactions in the heart. *Circ. Res.* **109**, 1082-1095.

Boura, E., Ivanov, V., Carlson, L.-A., Mizuuchi, K. and Hurley, J. H. (2012). Endosomal sorting complex required for transport (ESCRT) complexes induce phase-separated microdomains in supported lipid bilayers. *J. Biol. Chem.* **287**, 28144-28151.

Brenner, S. (1974). The genetics of Caenorhabditis elegans. *Genetics* **77**, 71-94.

Carlton, J. G. and Martin-Serrano, J. (2007). Parallels between cytokinesis and retroviral budding: a role for the ESCRT machinery. *Science* **316**, 1908-1912.

Cho, J. H., Oh, Y. S., Park, K. W., Yu, J., Choi, K. Y., Shin, J. Y., Kim, D. H., Park, W. J., Hamada, T., Kagawa, H. et al. (2000). Calsequestrin, a calcium sequestering protein localized at the sarcoplasmic reticulum, is not essential for body-wall muscle function in Caenorhabditis elegans. *J. Cell Sci.* **113**, 3947-3958.

Choudhuri, K., Llodrá, J., Roth, E. W., Tsai, J., Gordo, S., Wucherpfennig, K. W., Kam, L. C., Stokes, D. L. and Dustin, M. L. (2014). Polarized release of T-cell-receptor-enriched microvesicles at the immunological synapse. *Nature* **507**, 118-123.

Colombo, M., Moita, C., van Niel, G., Kowal, J., Vigneron, J., Benaroch, P., Manel, N., Moita, L. F., Théry, C. and Raposo, G. (2013). Analysis of ESCRT functions in exosome biogenesis, composition and secretion highlights the heterogeneity of extracellular vesicles. *J. Cell Sci.* **126**, 5553-5565.

Djeddi, A., Michelet, X., Culetto, E., Alberti, A., Barois, N. and Legouis, R. (2012). Induction of autophagy in ESCRT mutants is an adaptive response for cell survival in C. elegans. *J. Cell Sci.* **125**, 685-694.

Fourest-Lieuvin, A., Rendu, J., Osseni, A., Pernet-Gallay, K., Rossi, D., Oddoux, S., Brocard, J., Sorrentino, V., Marty, I. and Fauré, J. (2012). Role of triadin in the organization of reticulum membrane at the muscle triad. *J. Cell Sci.* **125**, 3443-3453.

Fyfe, I., Schuh, A. L., Edwardson, J. M. and Audhya, A. (2011). Association of the endosomal sorting complex ESCRT-II with the Vps20 subunit of ESCRT-III generates a curvature-sensitive complex capable of nucleating ESCRT-III filaments. *J. Biol. Chem.* **286**, 34262-34270.

Garrus, J. E., von Schwedler, U. K., Pornillos, O. W., Morham, S. G., Zavitz, K. H., Wang, H. E., Wettstein, D. A., Stray, K. M., Côté, M., Rich, R. L. et al. (2001). Tsg101 and the vacuolar protein sorting pathway are essential for HIV-1 budding. *Cell* **107**, 55-65.

Gokhin, D. S. and Fowler, V. M. (2011). Cytoplasmic gamma-actin and tropomodulin isoforms link to the sarcoplasmic reticulum in skeletal muscle fibers. *J. Cell Biol.* **194**, 105-120.

Hammarlund, M., Davis, W. S. and Jorgensen, E. M. (2000). Mutations in beta-spectrin disrupt axon outgrowth and sarcomere structure. *J. Cell Biol.* **149**, 931-942.

Hanson, P. I. and Cashikar, A. (2012). Multivesicular body morphogenesis. *Annu. Rev. Cell Dev. Biol.* **28**, 337-362.

Hobert, O. (2002). PCR fusion-based approach to create reporter gene constructs for expression analysis in transgenic C. elegans. *Biotechniques* **32**, 728-730.

Im, Y. J. and Hurley, J. H. (2008). Integrated structural model and membrane targeting mechanism of the human ESCRT-II complex. *Dev. Cell* **14**, 902-913.

Irion, U. and St Johnston, D. (2007). bicoid RNA localization requires specific binding of an endosomal sorting complex. *Nature* **445**, 554-558.

Jimenez, A. J., Maiuri, P., Lafaurie-Janvore, J., Divoux, S., Piel, M. and Perez, F. (2014). ESCRT machinery is required for plasma membrane repair. *Science* **343**, 1247136.

Jin, Y., Mancuso, J. J., Uzawa, S., Cronembold, D. and Cande, W. Z. (2005). The fission yeast homolog of the human transcription factor EAP30 blocks meiotic spindle pole body amplification. *Dev. Cell* **9**, 63-73.

Kamura, T., Burian, D., Khalili, H., Schmidt, S. L., Sato, S., Liu, W.-J., Conrad, M. N., Conaway, R. C., Conaway, J. W. and Shilatifard, A. (2001). Cloning and characterization of ELL-associated proteins EAP45 and EAP20: a role for yeast EAP-like proteins in regulation of gene expression by glucose. *J. Biol. Chem.* **276**, 16528-16533.

Kashyap, L., Perera, S. and Fisher, A. L. (2012). Identification of novel genes involved in sarcopenia through RNAi screening in Caenorhabditis elegans. *J. Gerontol. A Biol. Sci. Med. Sci.* **67**, 56-65.

Kerr, R. A. (2006). Imaging the activity of neurons and muscles. *WormBook* 1-13.

Kolotuev, I., Schwab, Y. and Labouesse, M. (2010). A precise and rapid mapping protocol for correlative light and electron microscopy of small invertebrate organisms. *Biol. Cell* **102**, 121-132.

Lange, S., Ouyang, K., Meyer, G., Cui, L., Cheng, H., Lieber, R. L. and Chen, J. (2009). Obscurin determines the architecture of the longitudinal sarcoplasmic reticulum. *J. Cell Sci.* **122**, 2640-2650.

Manière, X., Lebois, F., Matic, I., Ladoux, B., Di Meglio, J.-M. and Hersen, P. (2011). Running worms: C. elegans self-sorting by electrotaxis. *PLoS ONE* **6**, e16637.

Manil-Ségalen, M., Culetto, E., Legouis, R. and Lefebvre, C. (2014). Interactions between endosomal maturation and autophagy: analysis of ESCRT machinery during Caenorhabditis elegans development. *Methods Enzymol.* **534**, 93-118.

Maryon, E. B., Saari, B. and Anderson, P. (1998). Muscle-specific functions of ryanodine receptor channels in Caenorhabditis elegans. *J. Cell Sci.* **111**, 2885-2895.

McCullough, J., Colf, L. A. and Sundquist, W. I. (2013). Membrane fission reactions of the mammalian ESCRT pathway. *Annu. Rev. Biochem.* **82**, 663-692.

Mello, C. and Fire, A. (1995). DNA transformation. *Methods Cell Biol.* **48**, 451-482.
Mercker, M. and Marciniak-Czochra, A. (2015). Bud-neck scaffolding as a possible driving force in ESCRT-induced membrane budding. *Biophys. J.* **108**, 833-843.
Michelet, X., Alberti, A., Benkemoun, L., Roudier, N., Lefebvre, C. and Legouis, R. (2009). The ESCRT-III protein CeVPS-32 is enriched in domains distinct from CeVPS-27 and CeVPS-23 at the endosomal membrane of epithelial cells. *Biol. Cell* **101**, 599-615.
Olmos, Y., Hodgson, L., Mantell, J., Verkade, P. and Carlton, J. G. (2015). ESCRT-III controls nuclear envelope reformation. *Nature* **522**, 236-239.
Roudier, N., Lefebvre, C. and Legouis, R. (2005). CeVPS-27 is an endosomal protein required for the molting and the endocytic trafficking of the low-density lipoprotein receptor-related protein 1 in Caenorhabditis elegans. *Traffic* **6**, 695-705.
Schnorrer, F., Schönbauer, C., Langer, C. C. H., Dietzl, G., Novatchkova, M., Schernhuber, K., Fellner, M., Azaryan, A., Radolf, M., Stark, A. et al. (2010). Systematic genetic analysis of muscle morphogenesis and function in Drosophila. *Nature* **464**, 287-291.
Schuh, A. L., Hanna, M., Quinney, K., Wang, L., Sarkeshik, A., Yates, J. R. and Audhya, A. (2015). The VPS-20 subunit of the endosomal sorting complex ESCRT-III exhibits an open conformation in the absence of upstream activation. *Biochem. J.* **466**, 625-637.
Schwarz, J., Lewandrowski, I. and Bringmann, H. (2011). Reduced activity of a sensory neuron during a sleep-like state in Caenorhabditis elegans. *Curr. Biol.* **21**, R983-R984.
Schwarz, J., Spies, J.-P. and Bringmann, H. (2012). Reduced muscle contraction and a relaxed posture during sleep-like Lethargus. *Worm* **1**, 12-14.
Vaccari, T., Rusten, T. E., Menut, L., Nezis, I. P., Brech, A., Stenmark, H. and Bilder, D. (2009). Comparative analysis of ESCRT-I, ESCRT-II and ESCRT-III function in Drosophila by efficient isolation of ESCRT mutants. *J. Cell Sci.* **122**, 2413-2423.
Vietri, M., Schink, K. O., Campsteijn, C., Wegner, C. S., Schultz, S. W., Christ, L., Thoresen, S. B., Brech, A., Raiborg, C. and Stenmark, H. (2015). Spastin and ESCRT-III coordinate mitotic spindle disassembly and nuclear envelope sealing. *Nature* **522**, 231-235.
Warner, A., Qadota, H., Benian, G. M., Vogl, A. W. and Moerman, D. G. (2011). The Caenorhabditis elegans paxillin orthologue, PXL-1, is required for pharyngeal muscle contraction and for viability. *Mol. Biol. Cell* **22**, 2551-2563.
Watanabe, S., Richards, J., Hollopeter, G., Hobson, R. J., Davis, W. M. and Jorgensen, E. M. (2012). Nano-fEM: protein localization using photo-activated localization microscopy and electron microscopy. *J. Vis. Exp.* **70**, e3995.
Waterston, R. (1988). Muscle. In *The Nematode C. elegans*. (ed. W. B. Wood). pp. 281-335. Cold Spring Harbor, NY: Cold Spring Harbor Laboratory.
Webster, B. M., Colombi, P., Jäger, J. and Lusk, C. P. (2014). Surveillance of nuclear pore complex assembly by ESCRT-III/Vps4. *Cell* **159**, 388-401.